2024 European Control Conference (ECC)
June 25-28, 2024. Stockholm, Sweden

Automated Aquaculture Operations With Vessel-Mounted Robotic Arm: An Experimental Feasibility Study

Martin Albertsen Brandt*, Sverre Herland†, Martin Gutsch‡, Halgeir Ludvigsen‡ and Esten Ingar Grøtli*
*Department of Mathematics and Cybernetics, SINTEF Digital
†Department of Computer Science, Norwegian University of Science and Technology
‡Department of Ships and Ocean Structures, SINTEF Ocean

***Abstract*— Future aquaculture operations demand a higher degree of autonomy as new aquaculture locations are established in more exposed environments. In this study, we evaluate the feasibility of automating traditional fish farm operations through the utilization of a vessel-mounted robotic arm. We focus on a novel approach for automating the removal of deceased fish. Our work encompasses the technical design of a hose attachment and hook mechanism, simulations replicating realistic vessel and net pen motions, real-time prediction of fish cage collar positions using autoregressive models, and motion compensation control for the robotic arm. Scaled experiments indicate the feasibility of the proposed concept from a control perspective. This research contributes to the broader research challenge in robotics of managing interactions between a robotic arm mounted on a mobile platform and an environment that is also in motion.**

I. Introduction

Exposed aquaculture aims to cultivate fish in open water environments, primarily driven by the limited availability of suited sheltered locations and the higher costs associated with land-based farming. By venturing into open waters, exposed aquaculture endeavours to unlock untapped areas for fish cultivation. This approach seeks to capitalise on various expected advantages, such as enhanced water circulation, reduced risk of disease, and improved fish welfare. Moreover, exposed aquaculture holds the potential for sustainable expansion of the aquaculture industry, addressing the increasing global demand for seafood while simultaneously preserving natural ecosystems.

However, there are several considerations associated with transitioning to more exposed locations. When evaluating traditional fish farms comprised of multiple net pens, limited accessibility for conducting daily tasks emerges as a significant challenge. This issue stems from longer travel distances and harsher environmental conditions, resulting in shorter time windows for safe operation. Consequently, a fundamental overhaul of operations with a greater reliance on autonomy is necessary.

Collection of deceased fish is one of several daily operations pertaining to fish handling, which are currently done semi-manually [1]. Regulations state that deceased fish must be removed daily to limit the spread of potential disease [2]. Typically, the vessel is moored to the net pen, workers are brought on board the pen and a crane is used to handle the hose of the evacuation system used to transfer the deceased fish. Contact-free operations have been proposed as a potential solution to automate such work tasks. Contact-free operations entail carrying out tasks without the need to moor the vessel, instead relying on station-keeping next to the cage. This approach opens the possibility of redesigning certain operations to be partially automated without exposing personnel on the cage by using a crane or, as explored in this paper, a robotic arm.

Related work: Contact-free operations with a robotic arm was only recently proposed, see our previous work [3], resulting in limited related research for such operations. While dead fish removal has previously been considered using intervention remotely operated vehicles (ROVs) in rearing tanks [4] and net cages [5], the concept of automated dead-fish removal proposed here is novel. There are similarities to work on offshore crane control [6], vessel-to-vessel transfer [7], motion compensation of gangways [8], and robotic arms on vessels [9], yet they differ significantly from our proposed concept. In this work, motion planning and heave prediction are developed for a contact-free dead fish removal use case, tested experimentally on realistic vessel motions for typical operating conditions on exposed net pens. The simulations of vessel motions used here are previously described in [3], yet here, we also simulate the fish cage motions. Similar vessel simulations were also used in [7], although not as representative of environmental conditions at exposed aquaculture sites.

Contributions: The main contributions of the article can be summarized as follows:

- Introduction of a novel concept for automating dead-fish removal operations, enabling the operations to be conducted in a contact-free manner.
- Development of a technical design involving a hose attachment and hook mechanism, facilitating the experimental demonstration of the proposed concept.
- Simulations of realistic absolute motions of the vessel and net pen.
- Results from scaled experiments to assess the capability of a robotic arm mounted on a vessel to grasp objects in motion.
- Evaluation of the feasibility of the proposed concept, considering its practical applicability and effectiveness.

Outline: The article is organized as follows: Section II describes the simulations of vessel and pen collar; Section III describes the methods used to enable the pick-up and place-

down of a hose with a robotic arm in motion (i.e., motion prediction and trajectory generation). The experimental setup and necessary calibration procedures are introduced in Section IV, while the results are given in Section V. Finally, discussions and conclusions can be found in Section VI and Section VII, respectively.

II. Vessel simulations

A. Vessel model

For the presented simulations the service vessel AQS Loke[1] was used, as shown in Fig. 1 and presented in earlier work [3]. The vessel was chosen as an example of a modern aquaculture service vessel of sufficient size to be suitable for the simulated operation. Vessel information was provided by the vessel owner and was modelled without further modifications or optimizations of its operational performance.

Fig. 1. Aquaculture service vessel AQS Loke.

The vessel motion results are based on Response Amplitude Operators (RAOs) for the centre of gravity, calculated by the 2D linear strip theory vessel response code VERES [10], [11], along with the 3D potential vessel motion analysis software WAMIT[2]. The purpose of combining these tools for calculating the vessel response model is to utilize the frequency-dependent added mass and damping, as well as wave drift forces, from WAMIT, while VERES allows estimation of the viscous roll damping contributions.

As described in [3], the vessel motion calculations encompass the following parameters:

- One loading condition (see Table I).
- Zero speed.
- Wave heading of 150° (relating to port-side stern quartering waves).
- Wave periods calculated from $3\,\mathrm{s}$ to $60\,\mathrm{s}$.
- Linear 6 DOF motion RAOs[3].

TABLE I
Adapted loading condition.

Draught [m]	GM_T [m]	VCG [m]	R_{44} [m]	R_{55} [m]
2.20	8.27	2.90	5.36	6.09

[1]https://aqs.no/vessels/aqs-loke/
[2]https://www.wamit.com/

For the definition of the vessel load condition as presented in Table I, the midship draught, the transverse metacentric height GM_T, the vertical centre of gravity VCG, radii of gyration for roll R_{44} and pitch R_{55} for the vessel are specified.

B. Environmental model

The vessel motions were simulated in a colinear environment using the following environmental input data:

- Long-crested JONSWAP wave spectrum with significant wave height H_S, peak wave period T_P and peak enhancement factor γ, as given in Table II.
- Constant current speed of $0.5\,\mathrm{m/s}$.
- $100\,\mathrm{m}$ water depth.

TABLE II
Parameters of the wave spectra for the two simulations.

	H_S [m]	T_P [s]	γ
1	1.0	6.0	3.3
2	1.5	8.0	3.3

The wave height and period combinations of the chosen sea states represent a typical undisturbed wind sea, generally encountered in partly shielded coastal sea areas. The simulated relatively steep waves are most demanding for small vessels, as used in this study, with short roll and pitch resonance periods.

C. Simulations

The subsequent time-domain simulations were performed using SIMO [12] within the workbench and modeling environment of the SIMA platform [13]. The thrusters were modeled using SIMO 4.1 formulations for a conventional propulsion system and tunnel thrusters. For the tunnel thrusters, thrust losses due to thruster-hull and thruster-thruster interactions were included.

The robot base was positioned at the aft deck on the starboard side of the vessel, as seen in Fig. 2. During the simulation, the vessel was located next to the net pen. The pen motions were calculated separately using the fishery and aquaculture simulator FhSim [14]. The same wave realization was utilized in SIMO to calculate the vessel motions. The dynamic positioning (DP) controller used a point on the net pen collar as a reference position. The resulting footprint motions of the robot arm base and the point on the net pen collar are shown in Fig. 3.

III. Prediction and trajectory planning

A. Problem statement and related transformations

We consider the task of manipulating a moving object from a separately moving reference frame, in this case to perform pick and place of an object attached to a floating sea structure using a vessel-mounted robot manipulator arm. The task is illustrated conceptually in Fig. 2. We introduce the inertial frame $\mathcal{I}$, robot base frame $\mathcal{B}$, robot end effector frame $\mathcal{E}$ and target object frame $\mathcal{O}$.

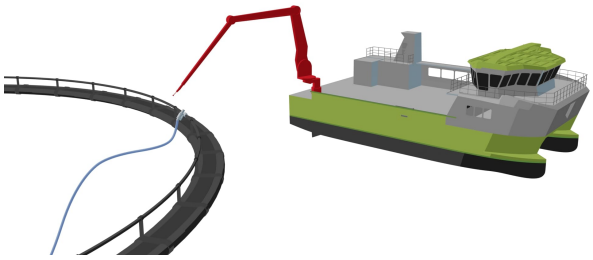

Fig. 2. Illustration of the proposed concept for dead fish removal. A vessel-mounted robot manipulator arm compensates for the relative motion of the net pen collar, and retrieves the hose onboard to perform the daily dead fish removal operation.

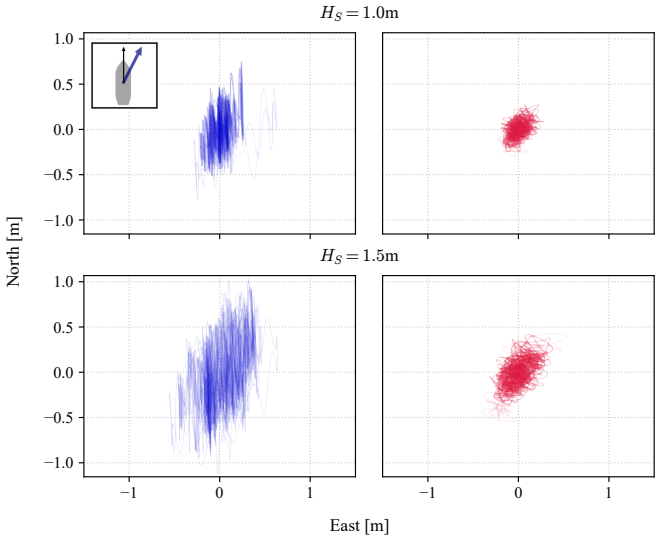

Fig. 3. Zero-centered footprints for vessel under DP (blue) and point of interest on fish cage collar (red) in North-East frame, for simulations with $H_S = 1.0\,\mathrm{m}$ and $H_S = 1.5\,\mathrm{m}$. The vessel heading (black arrow) is north, while the wave and current direction (blue arrow) is 30° north east, corresponding to stern quartering seas.

B. Trajectory planning

To complete a pick and place task while the robot base and target object are in motion, trajectory blending is used. This provides smooth motion between different frames, under the assumption that the relative motion between the frames is smooth. Specifically, linear interpolation is used for the desired end effector translation $p^\star$:

$$p^\star(t) = p_0(t) + \beta(s(t))(p_f(t) - p_0(t)), \tag{1}$$

where p_0 and p_f are the initial and target translations, respectively. A monotonically increasing blending function $\beta(s) : [0,1] \mapsto [0,1]$ is used to transition from the initial frame to the target frame. SLERP [15] interpolation is used for the desired end effector rotation quaternion $q^\star$:

$$q^\star(t) = q_0(t) \otimes \left(q_f(t) \otimes q_0(t)^{-1}\right)^{\beta(s(t))}, \tag{2}$$

where q_0 and q_f are the initial and target rotation quaternions, respectively, and $\otimes$ denotes the quaternion product. The quintic polynomial $\beta(s)$ with zero initial and final derivatives is used to blend between the frames:

$$\beta(s(t)) = 6s(t)^5 - 15s(t)^4 + 10s(t)^3. \tag{3}$$

$s(t)$ is scaled to interpolate between 0 to 1 over the duration of the current step, i.e., $s(t) = (t - t_0)/(t_f - t_0)$ for $t \in [t_0, t_f]$. We add additional substeps between the coordinate frames to achieve safe and controlled approach and retreat trajectories for the pick and place task.

C. Wave crest prediction using autoregressive models

Our method also incorporates a model for predicting the height of the next wave crest. Preliminary experiments highlighted a frequent issue, where due to latency within the control loop, the robot arm would often trail behind the hose and follow it down into the wave trough. To counteract this issue, a model was developed to forecast the wave's heave motion. The prediction of the next wave crest is used to guide the robot's actions with the intent to grasp the hose at the apex. This approach reduces the motion required by the end effector and also allows execution of the grasp when the speed of the hose is relatively low.

The vertical motion of the hose is modeled using an autoregressive (AR) model. AR models are capable of capturing the sinusoidal patterns anticipated in the heave motion and have previously been applied to similar problems [9]. Our model assumes that the vertical displacement z of the hose at any given time t is given by a linear combination of the previous K lagged displacements Δt, governed by learnable weights θ:

$$\hat{z}(t) = \sum_{i=1}^{K} \theta_i z(t - i\Delta t). \tag{4}$$

The model is continually refitted using L2-regularized least square regression to a moving window of the last H^- seconds of observed z values. To extrapolate into the future, we feed the predictions back into the model. This process is repeated until a forecast of the impending H^+ seconds of $\hat{z}$ is obtained. Lastly, a B-spline is fitted to the forecast, and its derivatives and their roots are examined to determine the time and height of the next crest.

The raw predictions of z are post-processed to obtain a more stable control target. Let t be the time we make a prediction, $\hat{z}^+$ be the predicted height of the impending crest at time $t^+ \in (t, t + H^+]$, and z^- be the height of the most recently observed crest at time $t^- \in [t - H^-, t]$. We then interpolate between the values of z^- and $\hat{z}^+$ based on where t falls in the interval $[t^-, t^+]$. In the first third, we use the value of z^-; in the last third, we use $\hat{z}^+$; and in the middle third, we linearly interpolate between the two. This prevents sharp discontinuities immediately after a crest is passed.

IV. Experimental Setup

A scaled experiment was developed to test the feasibility of the proposed automated dead fish removal task, see the experimental setup in Fig. 4. The previously introduced coordinate frames for the inertial, robot base, end effector

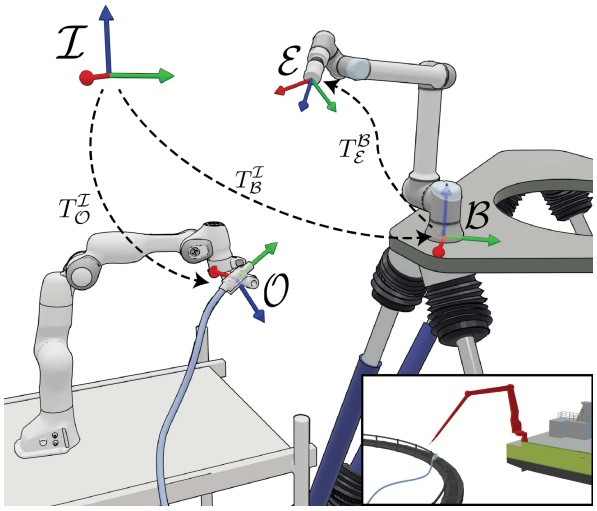

Fig. 4. Experimental setup with UR10e robot mounted on hexapod platform and Franka robot holding the hose. In the lower right corner the full scale analogue of the experimental setup is shown. The robot base frame $\mathcal{B}$, robot end effector frame $\mathcal{E}$, target object frame $\mathcal{O}$ and inertial frame $\mathcal{I}$ are also shown, and relevant transformations between these.

and target object frames are shown. In addition, the corresponding homogeneous transformations that map vectors in the base, end effector and object frames to the inertial frame, $T^{\mathcal{I}}_{\mathcal{B}}$, $T^{\mathcal{I}}_{\mathcal{E}}$ and $T^{\mathcal{I}}_{\mathcal{O}}$ respectively, are shown.

A Symétrie[3] Sirocco motion hexapod with a maximum payload of 2 tons was used to generate the scaled simulated vessel motions. A Universal Robots[4] UR10e robotic arm with a payload capacity of $10\,\mathrm{kg}$ and reach of $1.3\,\mathrm{m}$ was mounted on the platform and used to perform the pick and place task. The simulated motion of the point on the net pen collar was recreated using a 7 DOF Franka Emika[5] Panda robot with a payload capacity of $3\,\mathrm{kg}$ and reach of $0.855\,\mathrm{m}$. The collar motion trajectory was tracked using the franka-interface and frankapy [16] control stack. Both the Franka robot arm and the UR10e robot arm received commands at a frequency of $100\,\mathrm{Hz}$. The recreated motions using the hexapod and Franka robot arm were synchronized in time using the UDP-broadcasted start signal from the hexapod platform.

Froude similarity was used to preserve acceleration when scaling down the simulated vessel motions. The simulated motions for the vessel (hexapod) and point of interest on the fish collar (Franka robot) were scaled by a factor of $\lambda = 4.84$ in $\mathbb{R}^3$ and $\sqrt{\lambda} = 2.2$ in time, as in [3].

A mechanical attachment to a hose was designed and 3D-printed, which was connected to a "hand rail" end effector on the Franka robot with a hook, see Fig. 5 and Fig. 6. An OnRobot[6] MG10 magnetic gripper was used with the UR10e robot to grasp the hose and detect a successful grasp.

The considered task was broken down into a series of steps: approaching the collar point from above, grasping the hose attached to the handrail on the collar, moving the hose back onboard the vessel to perform the dead fish removal, and finally moving the hose back to the net pen and releasing it on the holder. A simplified version of this operation was demonstrated, without a hose attached to the hook.

[3]https://symetrie.fr/
[4]https://universal-robots.com/
[5]https://franka.de
[6]https://onrobot.com/

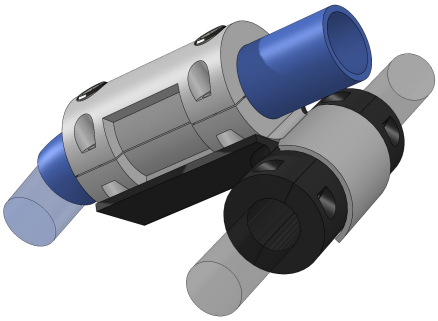

Fig. 5. Render of hose attachment with two connection points for the magnetic gripper and hook attached to the fish cage.

Fig. 6. End effector for Franka robot with hook for connecting the hose. Optical markers are added to the structure for motion tracking. The two bolts on the hose are used as connection points for the magnetic gripper on the UR10e robot manipulator arm.

To track the relevant frames in the environment a Qualisys[7] motion capture (MOCAP) system was used. Specifically, five Arqus 12 cameras were used, running at a frequency of $100\,\mathrm{Hz}$. Reflective markers were added to the robot base and Franka robot end effector, to track $T^{\mathcal{I}}_{\mathcal{B}}$ and $T^{\mathcal{I}}_{\mathcal{O}}$ in real-time. The desired grasp pose is then computed at every frame as

$$T^{\mathcal{B}}_{\mathcal{E}^\star} = {T^{\mathcal{I}}_{\mathcal{B}}}^{-1} T^{\mathcal{I}}_{\mathcal{O}^\star} T^{\mathcal{O}}_{\mathcal{E}^\star}. \tag{5}$$

Here $T^{\mathcal{I}}_{\mathcal{O}^\star}$ is the predicted pose of the hose at the next wave crest, generated by the heave predictor. $T^{\mathcal{O}}_{\mathcal{E}^\star}$ is the static transform between the hose attachment and the UR10e tool flange, which is calibrated a priori. The trajectory blending approach in Section III-B is used to interpolate back and forth between the initial pose of the robot manipulator and the desired transformations for grasping or releasing the hose.

[7]https://qualisys.com/

The hyperparameters for the crest prediction model are selected empirically from validation against a separate vessel motion dataset. We use an AR model with $K = 10$ autoregressive terms spaced $\Delta t = 0.1\,\mathrm{s}$ apart in time. The model is fitted to the last $H^- = 20\,\mathrm{s}$ of observed data and makes predictions at 20Hz with a horizon of $H^+ = 4s$. The sequence of predictions is smoothed using a second-order Butterworth filter with a critical frequency of $5\,\mathrm{Hz}$ and restricted so that the maximum speed of the control target cannot exceed $5\,\mathrm{cm/s}$. As a final safeguard, we also clamp the control target so that it can never go below the currently observed heave.

V. Results

For both datasets, generated with $H_S = 1.0\,\mathrm{m}$ and $H_S = 1.5\,\mathrm{m}$ waves respectively, a series of consecutive pick-and-place tests were completed. Statistics for the two series of tests are given in Table III. While for the $H_S = 1.0\,\mathrm{m}$ tests a success rate of 95.46% is reported, there is a significant decrease to 69.57% for $H_S = 1.5\,\mathrm{m}$. The failure modes, their possibly remedies and the ramifications for full scale field tests are discussed in detail in Section VI.

TABLE III
STATISTICS FOR THE TWO SERIES OF CONSECUTIVE TESTS.

H_S [m]	Total tests	Failures	Success rate [%]
1.0	22	1	95.46
1.5	23	7	69.57

Fig. 7 shows still images from the first pick and place sequence with $H_S = 1.5\,\mathrm{m}$, and provides an overview of the different steps of the task. In the second image the robot hovers directly above the desired grasp position on the "hand rail", which is estimated by the wave crest predictor, and waits for a safe window to grasp the hook. Similarly, once the robot reaches the desired position directly above the drop pose (in second to last image), the robot awaits a safe window to release the hook, i.e., at the next wave crest. Additional video material from the tests are made available[8].

For the same test, the control target derived from predicted crest height is shown with the actual wave height over the test duration in Fig. 8. We observe that the predictive model usually maintains a reasonable height. However, it dives down into the abnormally wide trough centered around $t = 17\,\mathrm{s}$. The abrupt drop can be explained by the small bump at the bottom of the trough. Because of its slight negative curvature, the bump is considered a crest by the model. Additionally, due to the flat region and the model's short context size (10 autoregressive terms - 1 second), the sharp rising edge at the far side of the trough is not anticipated sufficiently early. At this point, the clamping safeguard is activated and the control target follows the wave until the hose is dropped off around $t = 20\,\mathrm{s}$.

[8]https://youtu.be/USwijqDTdLM?si=K8jwl1RKfNPHOHIz

The desired and actual flange positions for the UR robot manipulator over the test duration are shown in Fig. 9. In Fig. 10 the corresponding tracking error is shown, given by the norm of the translational error and the arc length of the rotational error. The main component causing the tracking errors is the time delay in the internal robot controller. Thus the actual flange pose lags the desired pose, and the largest errors in Fig. 10 are seen for the steps in the pick-and-place task where the highest flange velocities are commanded, i.e., the states where the robot is moving towards or away from the target.

VI. Discussion

The results show how, for favorable weather conditions, it is feasible to perform pick and place operations to automate simple work tasks on the net pen using a robot arm on the vessel. Dead fish removal is considered here as an exemplary pick and place work task which may be automated, thus avoiding the need to transfer workers onboard the net cage. This may be extended to other operations, such as ROV launch and recovery, handling of the feeding tube, etc.

However, as seen in Table III, for larger wave height there is a significant increase in the number of grasp failures. All failures were due to a single failure mode: the magnetic gripper briefly connecting, detecting a magnetic contact, and then disconnecting due to a misaligned connection. This is caused by multiple factors. Firstly, the significant relative motion between the robot and the object means that time delay has a large influence on the accuracy of the grasping task, which must be precise to connect with the magnetic gripper. This is identified as a general challenge for manipulation tasks in moving frames where motions are not easily modeled or known a priori. The time delay is partially caused by latency in the motion capture system and additional computation delays. However, the main factor is the actuation delay in the UR10e robot. The robot's internal controller smooths the trajectory with a minimum time window of $30\,\mathrm{ms}$. This makes it more probable for the gripper to establish contacts which are not perfectly centered, and thus lose contact with the object.

Moreover, the developed magnetic connection mechanism was found to be particularly sensitive to motions in the xy-plane of the target object (see Fig. 4). It was seen that fast relative motions in xy-direction during grasping would often result in a misaligned connection and was considered the main contributor to the resulting failed grasps. In Fig. 11 the mean velocity in the xy-plane of the inertial frame around the moment of contact is shown separately for the successes and failures . While the sample size is small and there is a small roll offset between the inertial frame and the hose frame, the plot shows a tendency for higher xy velocity during contact to result in failed grasps. Other factors may influence these results, yet this indicates a deficiency in the design of the current magnetic connection mechanism to handle sideways motions. Because of this sensitivity it was deemed important for further development to develop a mechanical solution that

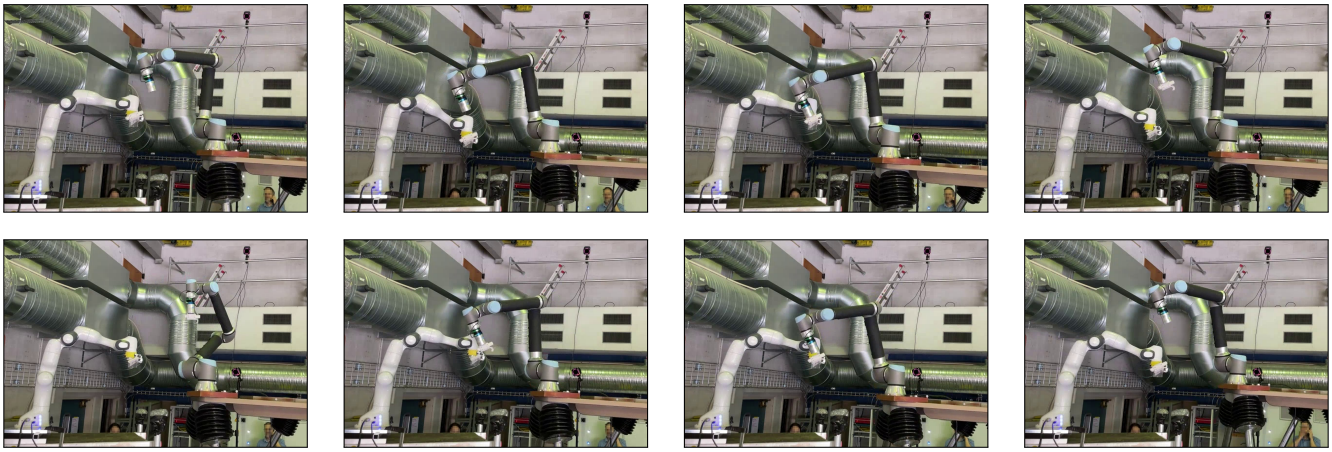

Fig. 7. Image sequence from pick and place task. Motion hexapod platform and Franka robot are moving according to scaled simulated vessel and fish cage motions, with $H_S = 1.5\,\mathrm{m}$ waves and scale factor $\lambda = 4.84$.

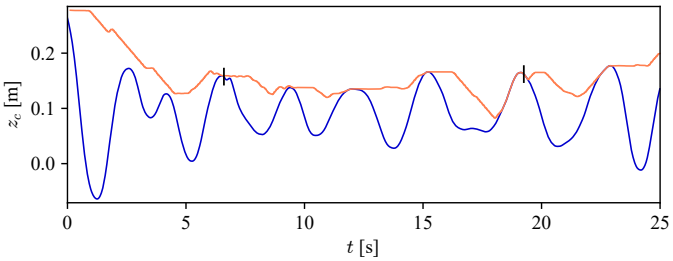

Fig. 8. Height of fish cage motion z_c (blue) and control target derived from predicted crest height $\hat{z}_c$ (orange). The two black markers indicate the two contact points when the hose is picked up and placed back down, respectively.

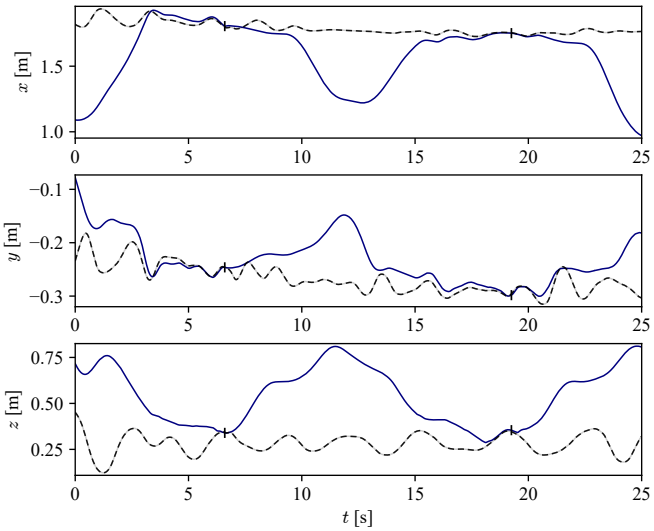

Fig. 9. UR10e robot flange position in inertial frame, in blue. Shown with the desired grasp pose for the point on the cage, in dashed. The two black markers denote the two contact points during the test, when the hook is picked up and placed back down, respectively.

passively guides the connection plate into a safe contact lock, instead of relying on accurate trajectory tracking alone.

It is seen that it is essential to develop technology for estimating the sea state and especially the motion of the targets on the net cage in real time to lower risk. While heave motion is the most critical to predict, we also observed a potential benefit of predicting the full 3D motion. As shown in Figure 11, failures were more likely to occur if the grasp coincided with high xy-plane velocity. Predictions of motion in the xy-plane would improve the tracking, which would reduce the relative shear motion between the gripper and the object. Alternatively, predictions could be used to initiate a grasp when the speed is expected to be low. The grasping strategy could also be improved by limiting pick and place to the rising edge of the current wave or by ignoring crests with height lower than a long-running statistic, e.g., estimated significant wave height.

The AR model presented here only employed 10 autoregressive terms, corresponding to a one-second window of wave motion. Consequently, it mainly made predictions based on information about the local curvature of the heave motion. When regular crests arrived with a period of around 2-3 seconds, this worked well. However, the short memory proved a potential issue during periods of less regular wave motion and longer spacing between the relevant crests. Additionally, low-frequency motions, such as those induced by the natural frequency of the cage structure, are very difficult to infer from just one second of data. This limitation can be overcome by widening the context window and including more autoregressive terms, but this will in turn introduce extra model parameters and demand more data, making online training impractical. Future work may explore higher-capacity models that have been pre-trained on a larger set of a priori collected data.

Lastly, multiple challenges must be addressed before the proposed system can be tested in field tests. As discussed in more detail in [3], structural and mechanical limitations of a full-scale robotic arm must be considered, as well as the requirements of the sensor system, e.g., based on motion reference units (MRUs) and fiducial marker tracking. Furthermore, handling of the hose itself is not considered. A

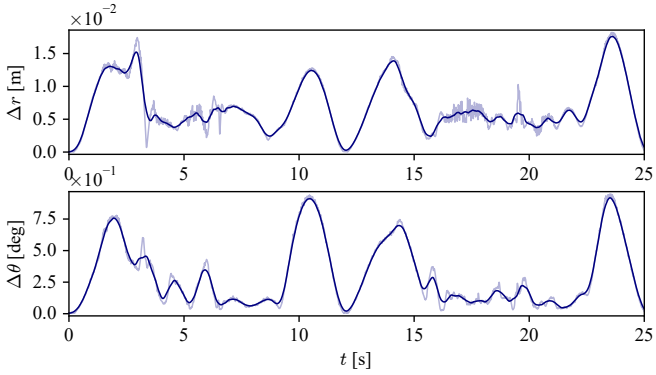

Fig. 10. Translational tracking error Δr and rotational tracking error $\Delta\theta$, between desired and measured end effector pose. Dark blue lines represent the 50-sample (0.5 s) moving average, the raw data is seen in the background.

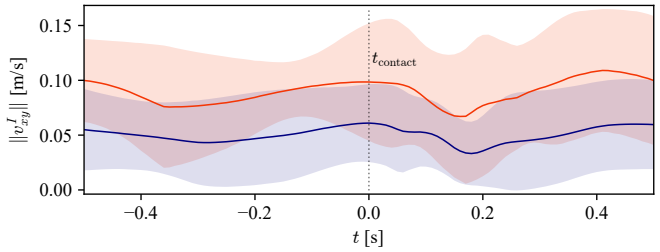

Fig. 11. Mean and standard deviation of norm of velocity of hook object in xy-plane of the inertial frame, shown independently for the successful pick and place trails (blue) and the failures (red). The data is centered around the time of contact t_{contact}.

mechanical solution, e.g., with a bracket or wheel must be developed to guide the hose safely as it is handled by the arm. Vessel design is another factor, as the service vessel used in this case study is designed for mooring, not station-keeping next to the net pen. Further work should therefore investigate optimal vessel design for the proposed automated operation, in terms of minimizing relative motions and possibly also the effect of the thrusters on the fish.

VII. Conclusion

In this paper, we have investigated the feasibility of performing aquaculture manipulation tasks with a vessel-mounted robot manipulator, thus avoiding mooring to the pen. A scaled experiment of an automated dead fish removal operation was presented, where a robot arm mounted on a hexapod platform grasps a hose on the net pen, emulated by a second robot arm. The hexapod platform and other robot arm moved according to simulated motions of an aquaculture service vessel station-keeping next to a net pen. Two series of tests were presented, where the robot on the vessel compensates for the relative motion guided by a heave prediction model, with success rates of 95.46% for $H_S = 1.0\,\text{m}$ and 69.57% for $H_S = 1.5\,\text{m}$. All failures could be traced to a single failure mode: poor robustness of the magnetic grasping. The results support the idea that doing manipulation tasks from the vessel-side with a robotic arm is feasible from a control perspective. At the same time, we see that as the sea state increases, the inaccuracies in calibration, motion estimation, and delay make high-precision grasping even more challenging. The findings emphasize the importance of a robust mechanical design of the attachment point of the dead fish removal system. Furthermore, limitations of a full-scale arm and the design of a sensor system were not treated in the study. These are, therefore, important next steps for realizing automated aquaculture manipulation tasks in full scale.

Acknowledgment

This work was funded by The Research Council of Norway (RCN) through the Center for Research-based Innovation Exposed Aquaculture Operations (RCN project number 237790) and Center for Research-based Innovation Safe Autonomous Ships for Sustainable Operations (RCN project number 309230).

References

[1] H. V. Bjelland, M. Føre, P. Lader, D. Kristiansen, I. M. Holmen, A. Fredheim, E. I. Grøtli, D. E. Fathi, F. Oppedal, I. B. Utne, and I. Schjølberg, "Exposed Aquaculture in Norway," in *OCEANS 2015 - MTS/IEEE Washington*, 2015, pp. 1–10.

[2] "Krav til opptak og håndtering av dødfisk i oppdrettsanlegg," https://www.mattilsynet.no/fisk-og-akvakultur/oppdrettsanlegg/krav-til-opptak-og-handtering-av-dodfisk-i-oppdrettsanlegg, accessed: 2023-10-31.

[3] M. A. Brandt, S. Herland, M. Gutsch, H. Ludvigsen, and E. I. Grøtli, "Towards autonomous contact-free operations in aquaculture," *Ocean Engineering*, vol. 282, p. 115005, 2023.

[4] B. O. A. Haugaløkken, O. Nissen, H. B. Amundsen, M. Føre, and E. Kelasidi, "Modelling and control of a 6 dof robot manipulator for underwater applications - aquaculture related case studies," in *OCEANS 2021: San Diego – Porto*, 2021.

[5] M. Vasileiou, N. Manos, and E. Kavallieratou, "Iura: An inexpensive underwater robotic arm for kalypso rov," in *2022 International Conference on Electrical, Computer, Communications and Mechatronics Engineering (ICECCME)*, 2022.

[6] V. W. Henriksen, A. G. Røine, E. Skjong, and T. A. Johansen, "Three-axis motion compensated crane head control," in *10th IFAC Conference on Control Applications in Marine Systems*, vol. 49, no. 23, 2016, pp. 159–166.

[7] S. S. Tørdal and G. Hovland, "Inverse kinematic control of an industrial robot used in vessel-to-vessel motion compensation," in *2017 25th Mediterranean Conference on Control and Automation (MED)*, 2017, pp. 1392–1397.

[8] L. Liang, Z. Le, S. Zhang, and J. Li, "Modeling and controller design of an active motion compensated gangway based on inverse dynamics in joint space," *Ocean Engineering*, vol. 197, p. 106864, 2020.

[9] P. J. From, J. T. Gravdahl, T. Lillehagen, and P. Abbeel, "Motion planning and control of robotic manipulators on seaborne platforms," *Control Engineering Practice*, vol. 19, no. 8, pp. 809–819, 2011.

[10] N. Salvesen, E. Tuck, and O. Faltinsen, "Ship Motions and Sea Loads," *Transactions of SNAME*, vol. 78, pp. 250–287, 1970.

[11] D. Fathi, "SHIPX Vessel Responses (VERES) - Ship Motions and Global Loads, User Manual," MARINTEK Report, 2012.

[12] "SIMO User and Theory Manual," https://sima.sintef.no/doc/4.4.0/simo/index.html, accessed: 2023-09-27.

[13] "SIMA workbench documentation website," https://www.sima.sintef.no/, accessed: 2023-09-27.

[14] K.-J. Reite, M. Føre, K. G. Aarsæther, J. Jensen, P. Rundtop, L. T. Kyllingstad, P. C. Endresen, D. Kristiansen, V. Johansen, and A. Fredheim, "Fhsim — Time Domain Simulation of Marine Systems," in *International Conference on Offshore Mechanics and Arctic Engineering*, 2014.

[15] K. Shoemake, "Animating rotation with quaternion curves," in *Proceedings of the 12th annual conference on Computer graphics and interactive techniques*, 1985, pp. 245–254.

[16] K. Zhang, M. Sharma, J. Liang, and O. Kroemer, "A modular robotic arm control stack for research: Franka-interface and frankapy," *arXiv preprint arXiv:2011.02398*, 2020.